Topological Analysis of Linear Polymer Melts: A Statistical Approach

Christos Tzoumanekas* and Doros N. Theodorou*

Department of Materials Science and Engineering, School of Chemical Engineering, National Technical University of Athens, Zografou Campus, 15780 Athens, Greece, and Dutch Polymer Institute (DPI), P.O. Box 902, 5600 AX Eindhoven, The Netherlands

Received March 29, 2006; Revised Manuscript Received April 19, 2006

ABSTRACT: We introduce an algorithm for the reduction of a computer generated atomistic polymer sample to an entanglement network of primitive paths. These networks are structural representations of the topology underlying a polymer melt. By examining network ensembles of polyethylene and *cis*-1,4-polybutadiene melts, we provide topological measures and statistical properties of primitive paths. We present the radial distribution function of entanglements and the distribution of the number of monomers between entanglements. A renewal point process that generates entanglement events along the monomer sequence of a chain is found to describe the statistics of detected topological constraints. We discuss chain thickness effects on topological measures and provide a method for detecting persistent chain contacts in melt configurations. A suitable scaling of acquired data leads to a unifying microscopic topological description of the melts studied.

1. Introduction

Polymer chains cannot cross each other. A successful conceptual framework embodying this principle at the molecular level is offered by the tube model.[1,2] The tube model postulates that the mutual uncrossability of polymer chains generates topological constraints (TCs), referred to as entanglements, which effectively restrict individual chain conformations in a curvilinear tubelike region enclosing each chain. Lateral chain motion is confined to the length scale of the tube diameter. Large-scale motion is promoted via reptation,[1] an effective one-dimensional diffusion of a chain along its tube axis. The latter provides a chain's coarse-grained representation that characterizes chain topology and is called the primitive path (PP). Edwards[3] regarded the PP as the shortest path constructed by keeping chain ends fixed while continuously tightening (shrinking) chain contour so that the resulting path has the same topology relative to other chains as the chain itself.[2,3] Applying this construction simultaneously for all chains[4,5] leads to a coarse-grained picture of a polymer melt that uncovers its large-scale topological superstructure. The latter is conceived[6,7] as a network of entangled PPs underlying the melt structure. The tube diameter d is assumed uniform[2] and corresponds to the mesh length of this network. Mesoscopic simulation models based on the above picture have been employed in rheological,[6] interface,[7] and glassy deformation[8] studies of polymers.

Entanglements dominate rheological and dynamical properties of large-molecular weight polymer melts,[1,2,13,22,23] as well as ultimate mechanical properties in the glassy state of these systems.[9−11] Their topological nature makes their direct experimental study difficult and their microscopic definition elusive.[12,25] A large number of phenomenological[13] and scaling[1,14−21] models, analytical,[2,22−24] experimental[13,22,25] and simulation[26−30,58,60] works have been devoted to the study of universal aspects of entanglement effects on melt dynamics and rheology. Other works have taken a static point of view where PP statistics have been studied analytically or in simulations, mainly in connection with the statistics of random walks in a regular array of obstacles.[1,4,31−33]

Recently, Everaers et al.[5] introduced a method of primitive path analysis (PPA) based on Edwards's definition of a PP. PPA applies a simultaneous contour reduction scheme to all chains of a computational sample, such that chain crossing is avoided and chain topology is conserved. The array of obstacles encountered by the shortest path of a chain is then microscopically determined from the shortest paths of other chains. Application of this method to FENE-type coarse-grained polymer chains has reproduced qualitatively and quantitatively[5] the packing length[18,19] scaling of the entanglement molecular weight M_e. An analysis of a coarse-grained model of bisphenol A polycarbonate[35] led to a very small value of M_e in agreement with experimental estimates and a direct determination of the plateau modulus from simulations. PPA has also been used[40,41] for investigating the entropic potential governing PP length distribution, as well as for determining M_e of glassy configurations[42] under equilibrium and macroscopic deformation.

In general, the static approach of microscopically determining PPs offers a promising basis for research on the general picture of entanglements invoked by the tube model. However, except for the work of Kröger[43] and a lattice-based[66] topological analysis, this idea has not been explored in a way that allows viewing TCs as discrete localized[58] objects in off-lattice geometries. In this work, we present a new methodology for reducing chains to shortest paths, such that TCs acquire a discrete localized nature by becoming the nodes of an entanglement network.[43] We apply this methodology to united-atom models of long-chain polyolefin and polydiene melts, which have been thoroughly equilibrated at all length scales using powerful connectivity-altering[26] Monte Carlo algorithms, and are known to capture very well structural, thermodynamical and dynamical properties of the real systems.[29,44−46] Preliminary accounts of our method[36,37] have appeared.

Mesoscopic views where a polymer melt is represented as an entanglement work (rubber analogy) have long been used as conceptual abstractions for the development of phenomeno-

* Corresponding authors. Address correspondence to the National Technical University of Athens. E-mail: doros@central.ntua.gr. E-mail: tzoum@central.ntua.gr.

10.1021/ma0607057 CCC: $33.50
Published on Web 05/25/2006

logical models[13] (transient network theory), and analytical theories[2] (slip-link models) in polymer physics. These views are guided by the rubberlike response of melts in viscoelastic experiments (rubbery plateau in the relaxation modulus), and the random walk (RW) statistics underlying the structure of flexible polymers. RW-like chain configurations, above some length scale, show a self-similarity, to which universalities and scaling laws detectable in physical properties can be attributed. When small length scale characteristics are ignored, the general problem of entanglement in polymers involves a system of interpenetrating RWs with a variable contour length density[14] imposed by chain thickness. The latter is specified by polymer chemistry. The polymer melts we study here consist of well packed RW-like chain conformations with a thickness corresponding to the chemistry of polyethelene (PE) and *cis*-1,4-polybutadiene (PB). Small length-scale characteristics have explicitly been taken into account in a manner that reproduces faithfully structural, dynamical, and thermodynamic properties[29,44−46] of these materials.

By analyzing the structure of PE and PB entanglement networks, we present microscopically determined distributions which describe statistically the topological state of flexible polymer melts. A suitable scaling of these distributions unveils a unifying topological description of polymer systems examined. We utilize a new algorithm, referred to as CReTA (contour reduction topological analysis), which is capable of reducing the atomistic configuration of a computational polymer sample to a network of corresponding PPs. Network nodes correspond to TCs experienced by individual chains, while network connectivity defines the underlying melt topology. Topological measures extracted from networks of entangled PE and PB melts are compared against corresponding experimental estimates. Quantitative agreement establishes these networks as meaningful structural representations of underlying melt topologies. In addition, we provide a stochastic interpretation of acquired topological data in terms of a point process which is able to describe the generation of TCs along a chain due to entanglement with other chains. The reported statistical properties of entanglement networks constitute a missing link for the construction of mesoscopic simulation models of polymer melts[6] and glasses[7,8] suitable for the prediction of rheological and large-deformation mechanical properties: One can use PP statistics in reverse-engineering fashion to construct entanglement networks obeying the mentioned distributions, for any flexible polymer.

The paper is organized as follows: In section 2 we present our general methodology. We follow a statistical approach, and we make an attempt to reveal "universal" signatures of polymer melt topology. Section 3 presents topological measures and several distributions describing PE, PB networks. We provide a renewal point process model for the generation of TCs along a chain and we discuss a simple interpretation. A dilute gas of entanglements is revealed by network radial distribution functions. We also investigate thickness effects and show a way to discriminate persistent TCs in melt configurations. In section 4, we provide a comparison of CReTA with recent similar approaches and discuss differences and similarities in the framework of microscopically determined PPs. Section 5 summarizes our conclusions.

2. Methodology—The CReTA Algorithm

Following Edwards's perspective and previous work,[4,5,43] CReTA provides a solution to the following geometric problem: "Given a set of uncrossable curved lines in space, reduce (shrink) continuously their contour lengths keeping their ends fixed, until the reduction process is blocked by topological constraints which organize into a network of quantifiable topology." The network is defined by a set of rectilinear segments (entanglement strands) coming together at nodal points (entanglements). Four strands belonging to two chains emanate from each entanglement point. Chain topology is specified by network connectivity. Network nodes can be reverse mapped to chain units (monomers) so that a correspondence between network and melt structure can be established.

For each polymer of interest, we examine an ensemble of statistically independent atomistic samples. The ensembles have been thermodynamically and topologically equilibrated at all length scales by previous Monte Carlo simulations[44−46] employing chain-connectivity altering moves. Through CReTA, atomistic configurations are reduced to networks, which are then analyzed to extract topological properties.

Connectivity altering moves[26] have proved very efficient in equilibrating long-chain polymer melts at all length scales. Employed initially[44,45,47] in Monte Carlo (MC) simulations, recently they have also been utilized[48] in molecular dynamics (MD) hybrid schemes, with considerable success in reducing the simulation time required for equilibration. By operating on the topological state space of conformations, such moves afford "topological relaxation" in MC simulations. Therefore, another advantage from their application to MC or MD is the potential supply of a multitude of topologically distinct computational samples for a polymer system under study. Such an ensemble can greatly facilitate statistical approaches to the topology of polymer melts, where large topological-type fluctuations of the network formed by the diverse tortuous conformations adopted by chains are possible. Additionally, as Hoy et al. have shown,[42] topological measures depend strongly on equilibration of chain structure at all length scales, so that proper equilibration is an essential prerequisite in topological investigations. Computer-aided topological studies following the spirit of Edwards's definition of PPs were proposed earlier[4] by Rubinstein and Helfand. However, it was only recently that a first attack to the problem[5] was presented, partly because of inherent difficulties in the computer simulation of long-chain polymer melts.[26,27]

CReTA implements random aligning string moves and hard core interactions. CH_x monomers are treated as united-atom hard spheres (beads) of diameter σ. Chains are represented as series of fused spheres, since in the atomistic polymer models considered here the skeletal bond distance ($\sim$1.5 Å) is smaller than σ ($\sim$4 Å). Periodic boundary conditions apply in all cubic sample directions. A string is defined as a set of $m \geq 1$ consecutive chain atoms. In each move, a string is randomly chosen and the string atoms are displaced to corresponding equidistant points on the straight line segment joining the atoms on either side of the string (see Figure 1). Chain ends are fixed throughout the process. To avoid chain crossing and preserve system topology, moves leading to overlaps between any string atom with any other atom belonging to a different chain are rejected. String moves leading to any bead displacement larger than σ are also rejected. Intrachain bead overlaps are permitted. These are sufficient conditions for preventing crossing when chains consist of fused hard spheres. m is randomly chosen between $1 + (i - 1)\Delta j$ and $i\Delta j$, with i initially set to 1 and Δj set to a small value. Accepted moves result in simultaneous reduction of chain contours and progressive shrinkage of unentangled loops to straight strands composed of fused spheres (see Figure 1). Rejected moves stem from either mutually blocked chain parts, which will lead to entanglements, or from

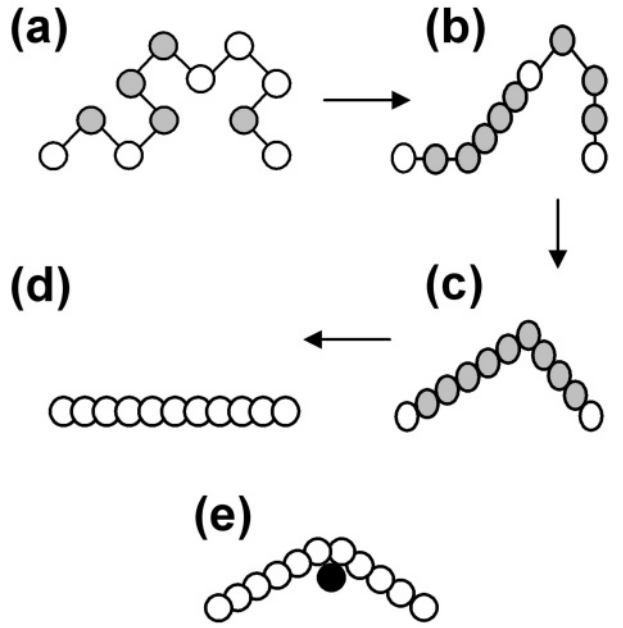

Figure 1. Aligning string moves of variable size employed in CReTA. The unentangled chain segment shown in part a becomes a straight segment by repeated string moves applied along its contour, as shown in parts a−d. In each figure, consecutive gray beads represent a randomly chosen string which becomes aligned in the next figure. In the united atom representation, a chain segment is composed of overlapping beads (fused spheres). Here, we have reduced bead sizes to clarify the course of aligning string moves. In part e, a segment of another chain perpendicular to the figure (denoted by a black circle) constrains the part c to d transition, so that successive string moves (not shown) result in the transition of part c to part e. Note that, if the perpendicular black chain segment is displaced in the course of aligning operations (which are applied stochastically on all chains), the white segment shown in part e will also be displaced and conform to the new position of the black segment.

"contacts" between unentangled loops, which will eventually disappear. To accelerate chain tightening, string sizes gradually increase through a heuristic $i \rightarrow i + 1$ conditioned loop. When chain contours are no longer diminishing, chain thickness is reduced by setting $\sigma \rightarrow g\sigma$, where $g < 1$, and the process starts anew. This aids in tightening meshed unentangled loops, which, although temporarily blocked, do not represent true TCs. Upon decreasing σ, to preserve the fused sphere sequence of chains (which ensures uncrossability) we place an auxiliary atom between successive skeletal atoms that have lost contact. Auxiliary atoms are taken into account in the final analysis by renormalizing the number of chain beads to the initial one. When a small predefined σ_f is reached, the whole procedure terminates (see also section 3.2). As shown in Figures 2 and 3 at this point, an underlying network structure of interpenetrating "zigzag" shaped PPs has been revealed. Further σ reduction to attain the infinitely thin-continuous line limit would be time-consuming and superfluous. Throughout this work we have used $g \sim 0.75$ and $\Delta j = 10$. These parameters influence the rate of convergence to reduced networks and not the final results. g should be close to unity.

The employed random aligning moves "eat up" contour curvature (chain slack), while at the same time respecting the relative TCs through hard core interactions. For example, if we think of a single line composed of straight segments (consisting of successive beads) connected by some U-shaped loops (consisting of beads as well) with the end beads held fixed, the action of CReTA will be more or less to first straighten the U loops (aligning moves acting on straight strands leave them as they are in 3D space) and thus transform the line to one consisting of straight segments connected by the reduced U loops. Further random aligning moves will eat up line curvature at places where the straight segments are connected obliquely, and so on, until the line becomes a perfectly straight one. Thus, our algorithm coarse-grains the line at progressively increasing length scales. At first it straightens small length-scale characteristics (the U-shape loops), and then it proceeds to larger length-scale characteristics (length scales involving successive straight strands with a kink between). In a real melt, however, the bodies of other chains block this coarse-graining at some places in space. To accelerate curvature reduction (which results in contour reduction), and thus to coarse grain contours at progressively larger length scales, string sizes have to conform to longer line segments during runtime. Thus, we increase string sizes when a prespecified condition is met (see below). Other conditions entering algorithmic implementation are related with the gradual decrease of chain thickness, which leads to a vanishing excluded volume for the whole system, and the addition of auxiliary atoms when σ is reduced.

To deal with the above conditions, we use a set of monitoring variables which store: (i) the contour length decrement of each chain; (ii) the largest separation of successive beads among all chains. This set is monitored whenever 1.25 string moves per monomer have been attempted on the average. Then, by checking against a set of prespecified conditions we decide about changes on parameters controlling program flow. Increase of string sizes is activated when all contour decrement variables take values less than 10^{-1}Å. This is implemented by increasing i in the loop mentioned above. When i reaches a maximum prespecified value, chain thickness is reduced and i is set to 1. Auxiliary atoms are added to the system when the monitored largest separation of successive beads becomes greater than the current value of σ. This choice is sufficient to ensure uncrossability, since, for hard-bead-type chains crossing is impossible[34] when bond lengths are less than $\sigma\sqrt{2}$.

Auxiliary atoms are added between all pairs of successive beads. We do this in order to avoid continuous monitoring of all bead separations and keep calculations simple. On the other hand, the addition of auxiliary atoms results in considerable system size increase during runtime. In our work this did not constitute a problem as the configurations analyzed were relatively small. A more efficient scheme for adding auxiliary atoms (e.g., locally, only between overstretched bonds) which avoids increase of system size is possible.

An efficient implementation of CReTA should deal with detections of potential bead overlaps of an attempted move, i.e., hard core interactions which take care of excluded volume. We use a cubic cell list. A search for possible overlaps is restricted into the cell containing a bead to be moved and the 26 surrounding cells. Since moves leading to bead displacements larger than σ are rejected, this scheme suffices if the cell edge is larger than σ. Intrachain hardcore overlaps are allowed; thus, self-entanglements and knots cannot be detected. One can introduce their detection in CReTA, if desirable, by following[34] Sukumaran et al. However, as these authors have shown and from our own experience with CReTA applications, occurrence and influence of knots in final results for the systems we studied is negligible. Here, we note that, due to periodic boundary conditions, chain segments belonging to different images of a chain are treated as parts of different chains.

A feature which greatly accelerates CReTA is the use of variable string size moves in conjunction with integer labels placed on all beads. Upon a successful string move, the labels of beads constituting the aligned string store the number of

aligned beads to the right of each string bead. We continuously update these labels during runtime. Attempted string moves that try to align already aligned strings can thus easily be detected and avoided. The convention used here is that a string move of m beads tries to align m beads to the right of a randomly chosen bead.

Starting from an average bead diameter taken from the equilibrated atomistic system, chain thickness is gradually reduced from σ to σ_f toward the final network state. One can start CReTA with chain thickness as thick as the desired final σ_f dictates.[49] With this choice, the simulation time will decrease considerably. However, we have chosen to reduce excluded volume gradually toward zero as a more faithful approach of attaining the vanishing thickness limit. These are the general characteristics of a CReTA implementation. Other details and tweaks will be described elsewhere. An enlightening visual perception of CReTA is provided by the videos added as supplemental information to this paper.

3. Results

3.1. Topological Measures. As shown in Figure 3, the resulting PPs consist of short pairwise blocked chain sections connected by straight strands of fused spheres (beads). By examining blocked regions and PP proximity we resolve PP "contacts" to pairs of neighboring beads. These specify pairwise associated TCs (beads) in the monomer sequence of their parent chains (see Figure 4). In addition, they represent effective spatial localization points of the TCs each chain is subjected to. By convention, throughout this work we interchangeably refer to these points as entanglements or TCs, in the sense that entanglements result from TCs. For the reduced chain conformations in the network we use the term PPs, in accordance with the Doi−Edwards definition[2] of the PP and with previous[5,34,43] work. Each PP is characterized by its ends and a set of entanglement points with specific spatial locations, monomer sequence indices, and pairwise associations to entanglement points on other chains. The whole structure can be reduced to a network, with nodal points (vertices) the entanglements, and edges the joining entanglement strands (ESs). Network connectivity specifies who is entangled with whom and in what sequence, and nodal positions specify where TCs apply. Topological analysis reduces then to an examination of network properties. The spacing between entanglements (network mesh) on the PP contour is measured both in number of monomers and in length units by calculating $\bar{N}_{ES}$ and $\bar{d}_{ES}$, the ensemble average of the number of monomers and end-to-end length, respectively, of an ES. Experimentally, entanglement spacing is mainly inferred either from the ES monomer length N_e, measured from the plateau regime[18] of the dynamic shear modulus, or from the tube diameter d measured as an intermediate dynamic length in neutron spin echo studies[12,25] of the dynamic structure factor. These are interpreted on the basis of the tube model, where PP conformations are considered as RWs and an ES is identified with the PP Kuhn segment.[2] Here, the relevant quantities[5] are the PP Kuhn length d and the number of monomers in a PP Kuhn segment N_e, defined through

$$d = \frac{R^2}{L}, \quad N_e = N\frac{R^2}{L^2} \tag{1}$$

where N denotes the average number of monomers in a chain and R^2 and L are the PP squared end-to-end distance and contour length, respectively. The latter are calculated here as ensemble averages over all chains present. By this "Kuhn mapping" approach, entanglement spacing emerges as the mesh spacing of an assumed uniform PP network of interpenetrating random walks.

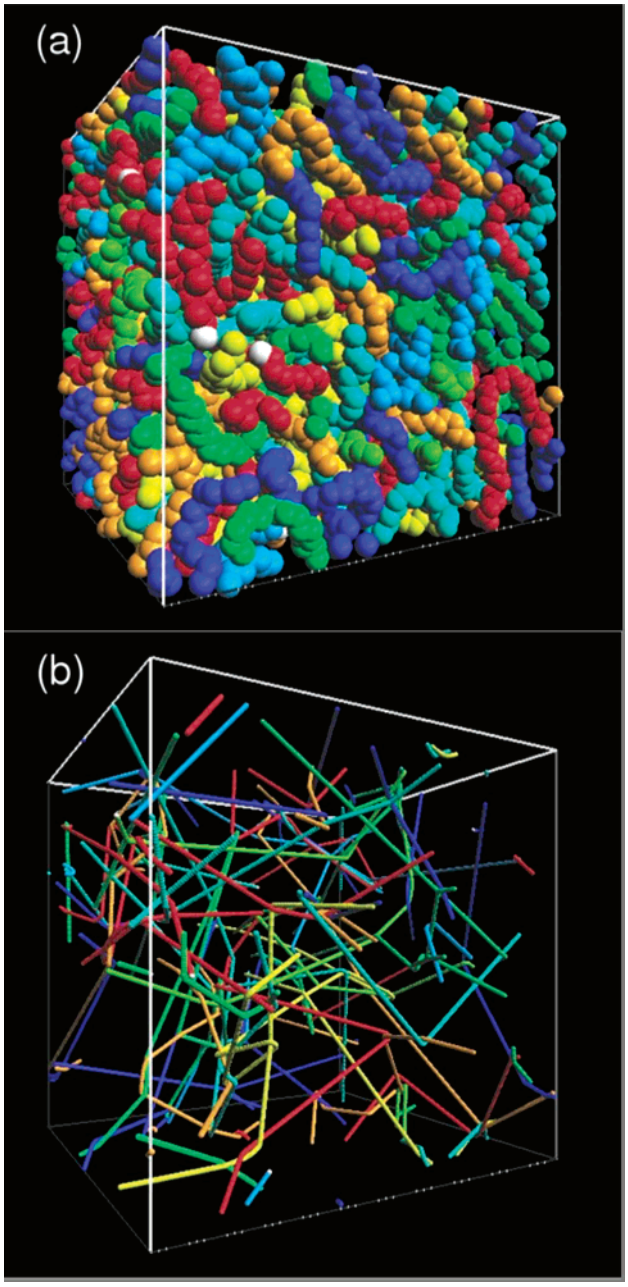

Figure 2. (a) Representative atomistic PE sample and (b) the corresponding reduced network.

Table 1 summarizes our results for $\bar{N}_{ES}$, N_e, $\bar{d}_{ES}$, d, the packing length p, and the density of the atomistic samples, along with corresponding experimental values. Results have been obtained with a $\sigma_f \simeq 0.5$ Å. p, an effective chain thickness[18,19] that controls coil packing, is defined as $1/(\rho_{ch}R^2)$, where ρ_{ch} is the number density of chains. It has been experimentally found[18,19] that p is a quantity which controls the degree of entanglement in polymer melts. Volumetric, structural, and conformational predictions for both polymers[44−46] are in excellent agreement with available experimental data. From the additional p data presented here, we conclude that the interplay between large-scale chain conformation and monomer packing is nicely captured by the atomistic ensembles. Turning to networks, PE samples of $N = 500$, 1000 display practically the same mesh values, indicating that well entangled samples possess a quantitatively similar underlying topology, independently of

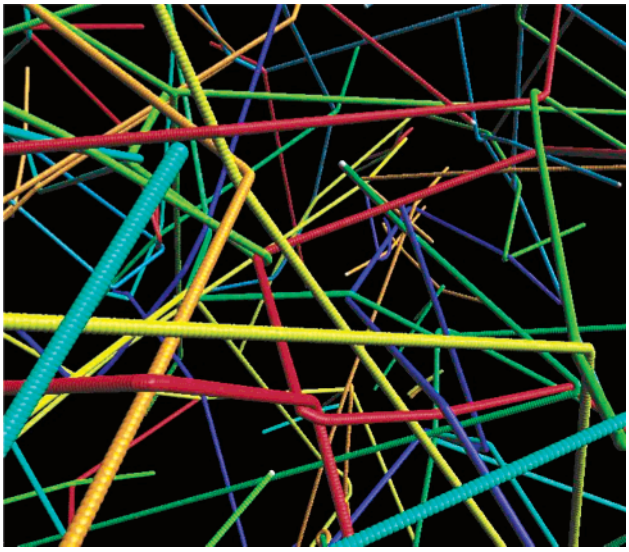

Figure 3. Closeup on PP network view of a PE melt.

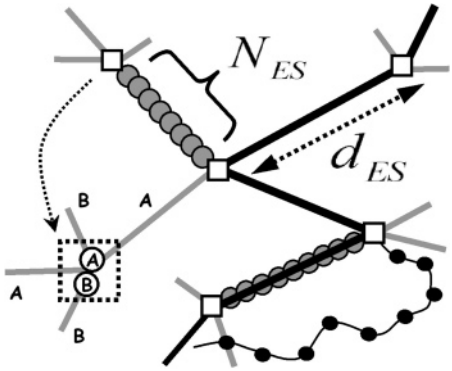

Figure 4. Schematic view of an entangled situation. White squares correspond to monomers (beads) where topological constraints (TCs) apply on chains. Gray circles correspond to monomers between successive TCs along a chain. The black line traces a succession of entanglement strands (ES) along the PP of a chain. TCs are pairwise associated by related beads (white circles A, B in the dashed square) along the monomer sequence of their parent chains A, B. Black circles denote monomer positions of an ES in the original atomistic configuration of the molten polymer. $\bar{N}_{ES}$ and $\bar{d}_{ES}$ are topological measures of the spacing (network mesh) between successive TCs along a chain, in number of monomers and length units, respectively. Throughout this work a monomer is defined as a CH_x united-atom hard sphere (bead) of diameter σ.

chain length. The small differences are attributable to the slightly different packing lengths. $\bar{N}_{ES}$, $\bar{d}_{ES}$, the network natural mesh spacing quantities, are much smaller than the corresponding PP Kuhn segment quantities N_e, d, with $\bar{N}_{ES} \sim 0.4N_e$ for both materials. Our analysis suggests that this is due to directional correlations between ESs along the same PP which decay exponentially with ES separation. That is, PP conformations are not RWs at the length scale defined by the network mesh size. At the Kuhn length scale, where PPs become RWs, N_e, d for both polymers are in good agreement with experimental estimations of the chain length between entanglements, as extracted from plateau modulus measurements. If we considered our systems as rubber networks of randomly coiled chains undergoing affine deformation, however, the small value of $\bar{N}_{ES}$ would imply a larger plateau modulus G_o than that found experimentally. Interestingly, in recent[6] Brownian dynamics simulations of 3D PP networks, the linear viscoelastic response of PB solutions is reproduced quantitatively only when an N_e of about half the experimental value is utilized, as found here for $\bar{N}_{ES}$. The discrepancy is rationalized[6] through the argument that one should invoke the phantom, as opposed to the affine, network model to estimate G_o, which for a tetrafunctional network would estimate approximately[6] half an N_e for the same G_o.

3.2. Chain Thickness Dependence. As we describe in section 2, CReTA implements a contour reduction process which is supported by a gradual decrease of chain thickness σ up to a very small predefined value σ_f. For a reduced network configuration of specified topology, as the one shown in Figure 2b, if we further decrease σ_f, then, at places where TCs apply, some extra space is created between chains which were previously in contact to each other. This extra chain "slack" is consumed by the contour reduction process, which results in further chain tightening. Hence, the PP contour length is smaller for smaller σ_f. Since chain ends are kept fixed and thus R^2 remains constant, the average PP contour length L and, through eq 1, N_e, d as well are then controlled by the chosen σ_f. A question that arises then, is: what is the dependence of L, N_e, and d on σ_f? In Figure 5, we plot these quantities as a function of σ_f for PE-1000, PB-1000. Data were obtained by starting the contour reduction process with a common chain thickness[45,46] $\sigma = 3.95$ Å for PE and PB, which was gradually reduced toward zero σ_f. Assuming the observed linear dependence $h(\sigma_f) = (A - B\sigma_f)$ of N_e on σ_f, the following relations hold:

$$N_e(\sigma_f) = Nh(\sigma_f)\,,\; d(\sigma_f) = R\sqrt{h(\sigma_f)}\,,\; L(\sigma_f) = \frac{R}{\sqrt{h(\sigma_f)}} \quad (2)$$

In Figure 5, we plot the above expressions with common A, B taken from linear fits to N_e data. Comparison with experimental data (see Table 1) becomes favorable with decreasing σ_f, particularly toward vanishing chain thickness. Extrapolating to this limit we get $N_e = 80.1$, $d = 38.2$ Å, for PE-1000, and $N_e = 190.6$, $d = 43.6$ Å, for PB-1000, in good agreement with published experimental data. Corresponding values for $\sigma_f = 0.5$ Å, presented in Table 1, differ from vanishing σ_f values by ~7% for N_e and ~4% for d. Throughout the paper, we have chosen to present results with $\sigma_f = 0.5$ Å, because, as explained in section 2, vanishing thickness calculations are computationally more demanding and do not offer a much better agreement with experimental data, nor a different viewpoint on the problem. Nonetheless, within CReTA, quantitative predictions necessitate the use of a small σ_f.

3.3. Entanglement Spacing Distribution. In Figure 6 we present the normalized distribution $P(n)$ of the reduced number of monomers N_{ES} in an ES, $n = N_{ES}/\bar{N}_{ES}$. We remind the reader that, throughout this work, the term monomer refers to a united atom (bead) and not to the chemical repeating unit. Actually, for the specific chemistry of PE and PB, N_{ES} corresponds to the number of skeletal carbon atoms between successive TCs along a chain.

Data from both materials superimpose on each other, falling on a master curve of the form

$$P(n) = \frac{bc}{c-b}(e^{-bn} - e^{-cn}) \quad (3)$$

with fitted values $b = 1.30$, $c = 3.78$. $P(n)$ corresponds to the molecular weight distribution of entanglement strands between successive TCs along a chain. In view of the large difference in $\bar{N}_{ES}$ and p, between PE and PB, the collapse of data suggests a universal character of $P(n)$ for linear polymers, although b, c, may depend on chemical details. The mean and

Table 1. Topological Measures of Reduced Entanglement Networks[a]

	N	$\bar{N}_{ES}$	$\bar{d}_{ES}$ (Å)	N_e	d (Å)	p (Å)
PE	500	28.3 ± 0.07	14.0 ± 0.04	75.1 ± 1.10 (61.4)	38.4 ± 0.54 (39.8)[b]	1.53 (1.69)
PE	1000	29.1 ± 0.07	14.1 ± 0.03	74.2 ± 1.05 (61.4)	36.6 ± 0.51 (39.8)[b]	1.65 (1.69)
PB	1000	80.9 ± 0.37	18.7 ± 0.07	178.7 ± 0.06 (173.8)	42.3 ± 0.01 (43.0)	2.59 (2.44)

[a] Entanglement spacing in monomer ($\bar{N}_{ES}$, N_e), and length ($\bar{d}_{ES}$, d) units of PP networks, and packing length p of the initial atomistic samples (equilibrated at $T = 450$ K (PE), $T = 413$ K (PB)). $\bar{N}_{ES}$, $\bar{d}_{ES}$ refer to the natural network mesh. N_e, d refer to the PP Kuhn mapping approach. Numbers in parentheses are experimental values from refs 18 and 19, unless otherwise indicated. The calculated polymer densities are 0.776 (0.766),[50] 0.778 (0.766),[50] and 0.867 (0.826) g/cm^3; the polydispersity indices are 1.053, 1.000, and 1.053; and the number of chains for each system studied are 16, 8, and 24 (top to bottom). Reported errors are standard errors of the mean. [b] Reference 12.

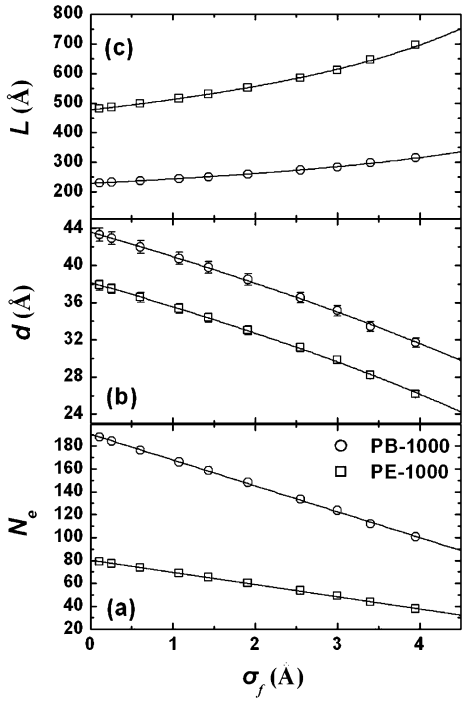

Figure 5. (a) N_e, (b) d, and (c) L, as a function of chain thickness σ_f, for PE-1000, PB-1000. Lines denote eqs 2, with common A, B, taken from linear fits to N_e data. Missing error bars have sizes less than or equal to symbol sizes.

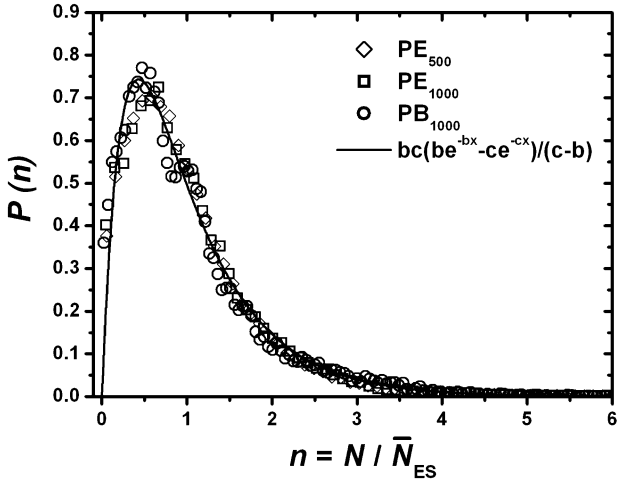

Figure 6. Normalized distribution of the reduced monomer distance between entanglements for the polymers of Table 1.

polydispersity index of n are given by

$$\bar{n} = \frac{1}{b} + \frac{1}{c}, \quad PI = \frac{\overline{n^2}}{\bar{n}^2} = 1 + \frac{b^2 + c^2}{(c+b)^2} \tag{4}$$

with PI = 1.62 for the fitted values of b, c. The distribution is broad with an exponential tail and in contrast with the tube model implies a nonuniform network mesh and large fluctuations in the number of monomers of an ES. An exponential distribution with a prefactor following a power law has been predicted[1,4,31−33] by simulations and calculations concerned with the number of Kuhn segments in an unentagled loop in lattice geometries. The origin of such fluctuations[4] and their effect on rheological properties, in the context of a Gaussian chain consisting of Kuhn segments, have recently been examined by Greco[51,52] and Schieber.[53]

3.4. Stochastic Model and Interpretation. We would like to be able to describe our data on the entanglement strand lengths in terms of a stochastic point process.[38] In such an approach, one considers the chain as a series of similar units (Kuhn segments, monomers, beads, etc.) and then draws a random number from a distribution of entanglement spacings, like $P(n)$, and places an entanglement event on a unit displaced forward by this spacing. The process is repeated until no more entanglements can be placed. TCs apply to the chain on entanglement sites, which are located on chain units where entanglement events have been placed. The kind of the point process, among other things, depends on the entanglement spacing distribution chosen. Since through CReTA we can locate monomer sites where TCs apply, a qualitative and quantitative point process approach is viable.

The simplest point processes, which serves as a basis of comparison with more complicated ones is the Poisson process.[38] In this process, the spacing between successive events is identically and independently distributed according to an exponential distribution. This is the case of maximum randomness, in the sense that instead of traveling along a chain of N units and placing entanglements according to an exponential distribution of mean spacing N_e, a realization of a Poisson process along the chain can be constructed by drawing (N/N_e) uniform random numbers from the interval [1, N], and then placing entanglement events on the units with corresponding indices. This would result in an exponential distribution for entanglement spacing, which by construction corresponds to completely uncorrelated entanglement positions along the chain. Thus, if the contour length of the chain constitutes the "volume" of this system, which is an open system since it exchanges entanglements with other chains (the surroundings), entanglements on this system can be described as a one-dimensional ideal gas in the grand canonical ensemble. The corresponding chemical potential fixes the average number of entanglement events N/N_e, while the distribution of the number of events will be a Poissonian. The chain is considered as a continuous line of length N here.

An exponential spacing for "stress points" along a chain has been assumed by des Cloizeaux in a series[54] of papers. Schieber[53] considered the 1D-ideal gas problem described above, for a Gaussian chain with a constant number of Kuhn segments in contact with a "bath" of entanglements. By fixing the corresponding chemical potential, he came up with an expo-

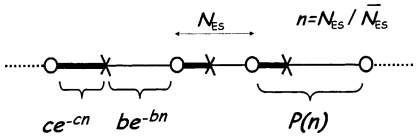

Figure 7. Schematic description of our stochastic interpretation of TC placement along the monomers (beads) of a chain, represented here through a continuous line. Circles denote beads where TCs apply along the chain, i.e., entanglement events. Crosses correspond to blocking events which protect previous beads (thick black segments) from entanglement events. An alternating Poisson process generates the alternating sequence of blocking and entanglement events. A renewal process generates the sequence of entanglement events (see text).

nential distribution for the number of Kuhn segments in an ES, which corresponds to a Poisson process of entanglement events. In our case, since chain units correspond to monomers, the exponential tail of $P(n)$ is the result of a similar stochastic process evolving on the monomer sequence space (along the beads) of a chain. However, in a Poisson process successive events can come arbitrarily close (the exponential distribution has a maximum at zero). On the other hand, it is meaningful to assume that, starting from an entanglement, the next entanglement requires a certain number of successive monomers (or length) to develop. Therefore, relative to a random distribution of entanglements, an extra monomer distance is needed in front of an entanglement before the next TC is observed. We characterize this extra chemical distance as an effective repulsion between successive TCs in the monomer sequence space of a chain. This kind of repulsion will become prominent close to and below the number of monomers in a Kuhn segment of the atomistic chain. This is evidenced in Figure 6 by the downturn and vanishing trend of $P(n)$ data as $n \rightarrow 0$.

A stochastic interpretation of our results can be given in terms of a renewal process, which is the generalization of a Poisson process. In such a process, event spacing is still identically, independently distributed, though with a distribution that is not exponential, cf. the normalized $P(n)$ presented here. Moreover, $P(n)$ is the convolution of two exponential distributions, namely be^{-bn} and ce^{-cn}. Thus, entanglement spacing in monomers can be considered as a random variable, distributed according to $P(n)$, which is the sum of two other exponentially distributed random variables. Accordingly, the underlying point process can be interpreted[38] as the result of two (uncorrelated) alternating Poisson processes with rates b, c, evolving on the monomer sequence space of a chain. The first process, with rate c, does not result in observable[38] events, such as the entanglement events observed as TCs along a chain. This process stochastically creates an unentangled monomer sequence in front of an entanglement, corresponding to the repulsion mentioned above. The related events act as "barriers" which protect previous monomers from entanglement events. The second process, with rate b, takes over when an unentangled sequence has been created and places an entanglement event on one of the following monomers. The outcome of the two Poisson processes is that entanglement spacing is distributed according to $P(n)$. Figure 7 shows a sketch of this idea.

Evidence that such a stochastic process can describe the placement of TCs along a chain is provided in Figure 8. There, we plot the distributions $P_i(n)$ of the reduced number of monomers constituting i successive ES along a chain, i.e., $n = \Sigma_{j=1}^{i} N_{ES,j}/\bar{N}_{ES}$ for PE-1000. $P(n)$ in eq 3 corresponds to the case $i = 1$. Since in a renewal process successive events are independently and identically distributed, these distributions can be calculated analytically from the i-fold convolution of $P(n)$ with itself (see the Appendix), which depends on n and the two

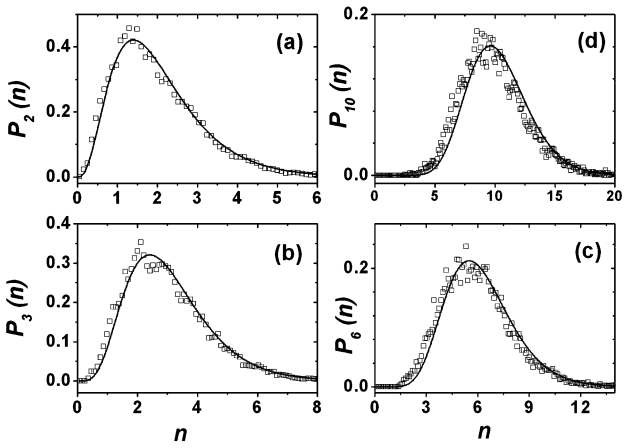

Figure 8. Normalized distributions $P_i(n)$ of the reduced number of monomers constituting i successive ES along a chain (see text). i is equal to 2, 3, 6, and 10 in parts a−d, respectively. Symbols correspond to data for PE-1000, while lines denote analytical predictions.

parameters b, c, as does $P(n)$. In Figure 8, we plot with symbols the $P_i(n)$ distributions for $i = \{2, 3, 6, 10\}$, as they were deduced from a topological analysis of our PE-1000 network data. Solid lines correspond to analytically predicted expressions for $P_i(n)$, with parameters b, c taken from our previous $P_1(n)$ fit (section 3.3) to PE, PB data. The invoked alternating Poisson process is able to follow the data. From the central limit theorem, as i increases $P_i(n)$ should asymptotically approach a Gaussian distribution, a feature that is evident in Figure 8.

Through our analysis, we have detected that successive entanglement spacings are not completely independent variables. They show small correlations which decay rapidly for larger strand separation along the chain. The analytically predicted distributions ignore these correlations, which result in small systematic deviations of the invoked process from the data. One can try to improve the stochastic description by including this kind of short-range correlations.[38] However, the simplicity of the invoked process, the interpretation that can be given, and the good agreement with the data led us to ignore them here. Furthermore, analytic expressions for $P_i(n)$ invoke a continuous point process, while the monomer sequence space of a chain is a discrete system. The presented analysis concerns only the inner strands of the chains. End strands can also be described through $P(n)$, albeit with slightly different b, c.

Note that the coefficient of variation (COV) of $P(n)$, defined as the ratio of the variance of the distribution over the squared mean, is 0.62, with b, c taken from section 3.3. Thus, $P(n)$ is less dispersed than an exponential distribution which has a COV equal to one. In the language of point processes, an event spacing distribution with a COV less than one[38] indicates a process which is qualitatively more regular (less clustered) than a Poisson process. The latter would result in a polydispersity index equal to 2.

3.5. Distribution of the Number of Entanglements (TCs) Per Chain. Figure 9 presents the normalized distribution $P(Z_{ES})$ of the number of entanglements (TCs) per chain, Z_{ES}, for PE-1000 data. The mean and the standard deviation of $P(Z_{ES})$ are $\bar{Z}_{ES} = 33.7$ and $\sigma_{Z_{ES}} = 5.15$, respectively. The average number of PP steps per chain at the length scale of the network mesh is $\bar{Z}_{ES} + 1$. As we have seen in the previous section, a renewal process generating entanglement events along a chain can provide a stochastic model in good agreement with available data. Then, a general prediction of renewal[38,39] theory, about the limiting distribution of Z_{ES} as $N \rightarrow \infty$, is that Z_{ES} is

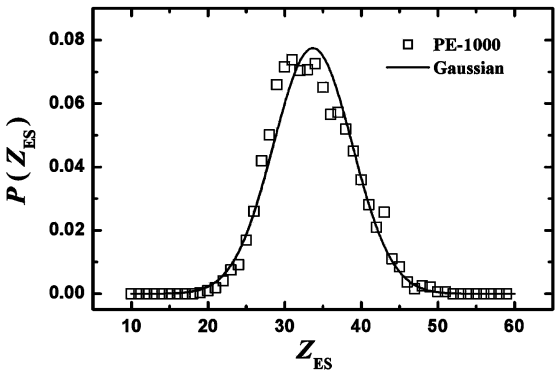

Figure 9. Normalized distribution $P(Z_{ES})$ of the number of entanglements (TCs) Z_{ES} per chain. Symbols correspond to PE-1000 data. The solid line is a Gaussian with the same variance and mean of PE-1000 data.

asymptotically normally distributed with mean $\bar{Z}_{ES}$ and variance $\sigma_{Z_{ES}}^2$,

$$\bar{Z}_{ES} \to N/\bar{N}_{ES},\ \sigma_{Z_{ES}}^2 \to \sigma_{N_{ES}}^2 N/\bar{N}_{ES}^3 \tag{5}$$

where $\sigma_{N_{ES}}^2$ is the variance of N_{ES}. This is also true in the case of a Poisson process of entanglement events, when $\bar{Z}_{ES}$ is large. The solid line in Figure 9 shows a normalized Gaussian with mean $\bar{Z}_{ES}$ and variance $\sigma_{Z_{ES}}^2$ taken from PE-1000 data (not a fit). It is clear that $P(Z_{ES})$ deviates from a Gaussian, although it has a similar shape. The source of this small difference is the existing short-range correlations between successive event spacings described in the previous section and the fact that the asymptotic limit corresponds to much longer chains than the ones examined here.

From the form of the asymptotic mean and variance it follows that[38,39] for the limiting distribution of Z_{ES}:

$$\frac{\sigma_{Z_{ES}}^2}{\bar{Z}_{ES}} \sim \frac{\sigma_{N_{ES}}^2}{\bar{N}_{ES}^2} \tag{6}$$

For a Poisson process, which is a renewal process with an exponential distribution of event spacing, the above relation becomes exact with both terms being equal to one.[39] Relation 6 connects the statistics of entanglement event spacing N_{ES}, and number of events Z_{ES}, in the asymptotic limit $N \to \infty$ of a renewal process. For PE-1000 data, $\sigma_{N_{ES}}^2/\bar{N}_{ES}^2 = 0.62$ while $\sigma_{Z_{ES}}^2/\bar{Z}_{ES} = 0.79$, an indication that we are still far from the asymptotic limit. Considering the complexity of the problem, the renewal process model is able to describe the general picture of TCs derived from an analysis of our data very well.

3.6. Spatial Distribution of Topological Constraints. In this section we examine spatial correlations between network nodal points. Nodal coordinates are assigned to the midpoints between beads specifying pairwise associated TCs on their parent chains (see Figure 4). This operation slightly distorts PP conformations, since what remains is a reduced network defined by a set of nodal points connected through straight segments of zero thickness.

In Figure 10, we present the total and partial radial distribution functions (RDFs) of entanglements vs $r' = r/\bar{d}_{ES}$, the spatial distance r reduced by the average network mesh length. Partial RDFs correspond to correlations between different pair types[55] of binary entanglements. As shown in Figure 11, RDF-0 curves correspond to entanglements which are "spatial neighbors" , i.e., all four chains passing through them are different. RDF-1 and RDF-2 curves correspond to entanglements at any distance

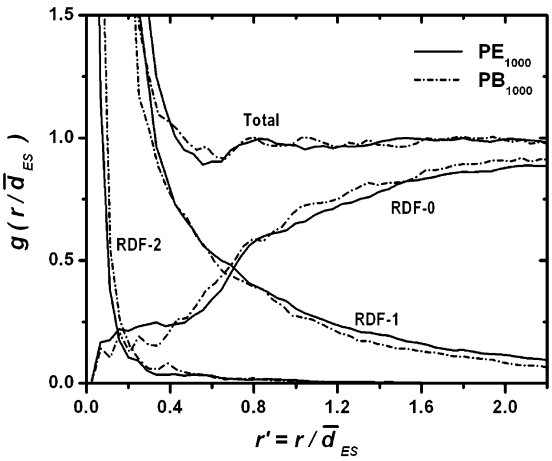

Figure 10. Total and partial RDFs of PE-1000 (solid) and PB-1000 (dot-dashed). Partial RDFs depict correlations between different pair types of binary entanglements. Each case is sketched in Figure 11.

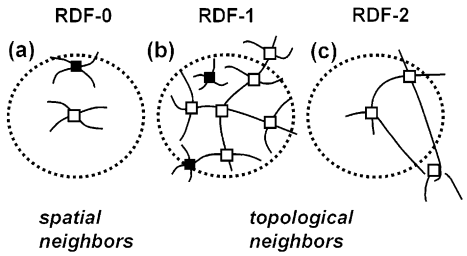

Figure 11. Different types of pairs of binary entanglements. Spatial neighbors are entanglement pairs where all four chains passing through them are different (a). Topological neighbors are entanglement pairs at *any distance* which are connected by one (b) or two (c) common chains passing through them. In all three sketches, black(white) squares denote spatial(topological) neighbors to the entanglement located at the circle center. Note that in parts b and c, it is possible for entanglements along the same chain to approach each other very closely in space, even if the number of entanglement strands between them is greater than one (depicted in case c).

that are "topological neighbors" , i.e., connected by one or two common chains, respectively, passing through them. Apart from some minor differences, the curves for PE, PB superimpose on each other. Therefore, the spatial network nodal correlations stemming from the underlying topologies of the PE, PB melts are similar when scaled accordingly.

The total RDF implies that in the range $r' \geq 0.8$ network structure can be described as an ideal dilute gas[9] of entanglements, with short-range correlations occurring at smaller r. Specifically, RDF-1,2 decay like $r^{-\nu}$ with ν taking values between 1.3 and 1.45. If we recall1 that the pair distribution function for a single ideal chain decays like $1/r$, we expect that RDF-1,2 display an r dependence which corresponds to single-chain-type contributions to the total RDF. Here, by "chain" we mean a series of sticks and nodes which define a PP in the reduced network. However, as illustrated schematically in Figure 11, RDF-1,2 capture contributions from two PPs, which, as explained in section 3.1 are not ideal chains at the length scale defined by the network mesh. Furthermore, in reduced network representation the PP system is polydisperse, with a distribution of molecular weights given by eq 3 and a polydispersity index given by eq 4. For these reasons, the value of ν departs from unity.

The fact that RDF-0 curves are below RDF-1 curves for $r' \leq 0.7$ indicates that, in the region around and near an entanglement, topological neighbors persist and spatial neighbors cannot easily penetrate. This is a kind of correlation-hole[1] effect.

CDV

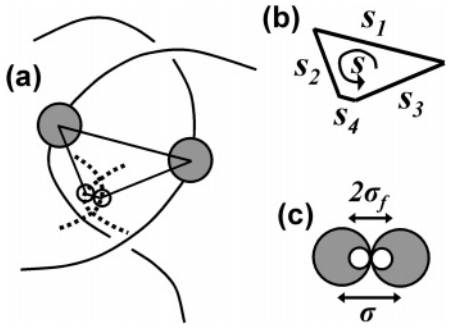

Figure 12. Two-dimensional schematic view of a TC. (a) Beads which define a TC are shown as gray(white) circles in their corresponding melt(reduced network) positions. Bead diameter is $\sigma(\sigma_f)$ in the melt-(network) state, with $\sigma_f \ll \sigma$. Atomistically represented chains are shown as solid curves, and PPs as broken curves. (b) Total length s of the closed path formed by the four straight-line segments s_i which connect melt and network bead positions. (c) Configuration of minimum s length, $s_{min} = 2\sigma$ (see text). In general, s_i vectors are not coplanar. Note that chain contact between PPs (in reduced network configurations) does not necessarily imply chain contact in corresponding atomistic melt configurations.

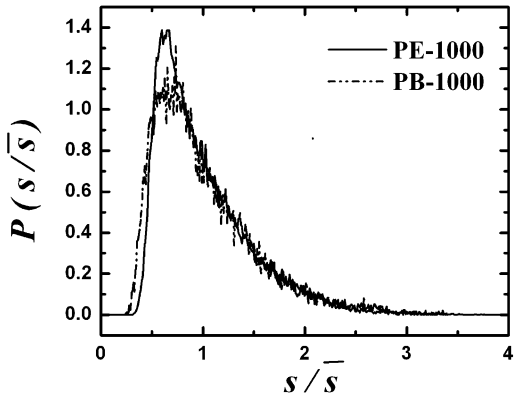

Figure 13. Reduced normalized distribution of s.

Spatial neighbors populate primarily the region beyond $r' \sim 0.7$ around a node, where RDF-0 curves overpass RDF-1 curves. RDF-2 curves correspond to pairs of chains intertwined through two entanglements and decay rapidly with r'. Intertwining results in closely spaced entanglements and is highly improbable at large distances. The combined action of partial correlations results in an ideal gas environment around a network node at length scales larger than the average network mesh size $\bar{d}_{ES}$.

3.7. Mapping TCs back to the Atomistic Level. The contour reduction process displaces beads from their melt positions to corresponding reduced network positions. Within CReTA, each bead has a specific position both in the molten and in the reduced network state. Since in our work TCs emerge as binary entanglements and are assigned to pairs of specific beads along their parent entangled chains, we can inquire on bead positional correlations between melt and reduced network states. As a measure of these correlations, we introduce the total length s of the closed path formed by joining the four straight-line segments s_i connecting melt and network bead positions (see Figure 12). The minimum possible value of s, s_{min}, equals 2σ, as shown schematically in Figure 12. This is the case when the beads defining a TC were in contact in the molten state; in the course of contour reduction process (which gradually reduces bead diameter from σ to σ_f), beads have remained in contact in reduced network configurations through displacements along the straight line joining their centers in the melt state.

Figure 13 presents $P(s/\bar{s})$, the reduced normalized distributions of s divided by its mean value $\bar{s}$, for PE-1000, PB-1000. $\bar{s}$ is 22.3 Å for PE-1000 and 29.4 Å for PB-1000. A common $\sigma_f = 0.5$ Å has been used for the final thickness of PE-1000, PB-1000 reduced networks. Curves in Figure 13 rise steeply from zero at a $s_{min}/\bar{s}$ value which is somewhat smaller for PB, and is approximately equal to $2\sigma/\bar{s}$ for each polymer. Note that the average σ for the atomistic PB samples[46] is 3.7 Å, vs 3.95 Å for atomistic PE.[45] Peak values are different, due to this difference in $2\sigma/\bar{s}$ (the distributions are normalized). Results, however, are superposable between the two polymers in the tail region. $\bar{s}_1$ is ~43% of $\bar{s}$, while the $\bar{s}_4$ contribution to $\bar{s}$ is negligible and vanishes in the limiting case of infinitely thin PPs. Peaks are located at $s \sim 0.65\bar{s}$.

In general, as chain slack (stored length) is gradually removed from the system, TCs around and to the left of the peak appear first, while TCs associated with the tail appear when a larger amount of chain slack has been consumed. There exist also TCs which form early in the contour reduction scheme, but are more or less rigidly displaced toward their final network locations as further chain slack is consumed.[56] TCs associated with an s to the left of the peak in Figure 13 correspond to chain contacts in the molten state which (i) define a TC in the reduced network configurations, i.e., also constitute contacts between PPs, and (ii) are not displaced over large distances in the course of the contour reduction process, i.e., are "local" *in the melt* configurations in comparison with TCs associated with a larger s. These TCs may define persistent contacts[15,57−59] between chains which influence dynamics a lot more than other TCs. "Local" TCs in melt configurations result in chain contacts which are expected to show larger "lifetimes" on the average (and thus be persistent) in comparison with numerous other contacts between chains. One can think that a "local" TC will act as a slip-link which will create a persistent contact between two chains. As long as this slip-link is active, thermal fluctuations will "slide" it along the two chain backbones, so that, at different time instances, the related chain contact may be associated with a different monomer pair along the monomer sequences of the two chains.

The features seen in Figure 13 suggest that all TCs are not equivalent in the way they restrict chain conformations. For example, in the time domain a chain could experience TCs to the left of the peak much sooner than TCs associated with the tail of the distribution. Furthermore, upon deformation some TCs could be fully "activated" only in the nonlinear regime. However, we note that only when all chain slack has been removed from the system, and thus all TCs have been revealed as PP contacts in the networks, does the average contour length L computed from PPs through eq 1 lead to quantitative estimates of N_e, d which are in good agreement with experimental data.

In this respect, the reduced networks under study reveal the maximum number of TCs restricting chain conformations through direct PP contacts in reduced network configurations. Within CReTA it would be possible to stop contour reduction at a stage where the average L' of reduced chains would be larger than L in the final reduced network state; that is, to leave some chain slack in the system. In this case "Kuhn mapping" would give smaller values for both N_e and d. Then, through eq 1, L' could be adjusted so that Kuhn mapping would provide an N_e equal to $\bar{N}_{ES}$. In these reduced configurations PPs would look more like "floating curves" in space than like kinky lines. Some PP contacts, while present in reduced networks where all chain slack has been removed, would be absent in configurations with remaining slack. However, topological interactions associated with conformational space restrictions and related with these PP contacts, would still exist even in their absence.

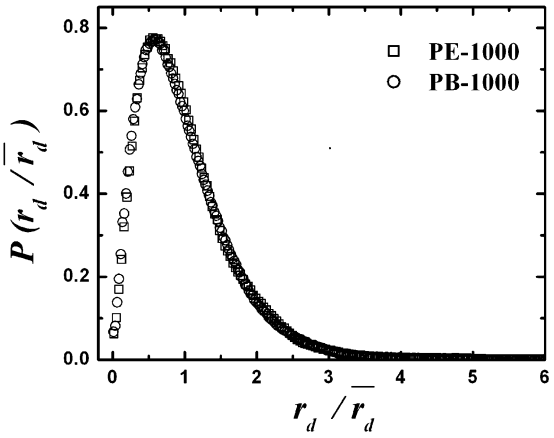

Figure 14. Reduced normalized distribution of the *normal distance* r_d of a bead's melt position from the corresponding network straight segment (PP strand) carrying this bead.

Another quantity we have analyzed is the average *normal distance* $\bar{r}_d$ of a bead's melt position from the corresponding reduced network straight segment (ES) carrying this bead (see Figure 4). Figure 14 presents the normalized distribution $P(r_d/\bar{r}_d)$ for PE-1000, PB-1000 melts. Superposition is perfect due to the very good statistics attained by the calculation (all beads over all samples). In a sense, this distribution determines the statistics of the radial profile of melt conformations around PP strands. $\bar{r}_d$ values are 7.1 Å for PE-1000 and 10.0 Å for PB-1000, close to $\bar{d}_{ES}/2$ for both materials. The root-mean-square (rms) value of r_d is also roughly half the rms value of $\bar{d}_{ES}$. Thus, chain conformations fluctuate around computed PP conformations on a length scale defined by the "natural" mesh of generated networks, as it is measured through $\bar{N}_{ES}$, $\bar{d}_{ES}$.

4. Comparison with Similar Approaches

CReTA has similarities and differences with other recently developed methods aiming at the topological analysis of polymer melts. All methods apply a contour reduction scheme simultaneously to all chains up to the level that TCs block further contour reduction. Contour reduction is actually a coarse-graining scheme. The goal is to reveal a coarse-grained chain conformation which is topologically compatible with various conformations that a chain can adopt in the environment of other chains. The adopted coarse-graining scheme is responsible for final reduced states, i.e., PP conformations, PP contour length fluctuations, PP Kuhn length, density of TCs, distribution of entanglement spacings, etc. All approaches ignore self-entanglements. Their contribution to final results has been considered in ref 34 and has been found to be negligible. Below we attempt a summary of general differences and similarities between CReTA and alternative approaches, which would be of value at the current stage of research. All approaches invoke a static-type coarse graining. The time domain is left out, although PPs could also be defined through a temporal coarse graining. Temporal coarse graining may be included in the definition of PPs too; reptation is connected with this picture, and there has been research[60] toward this direction.

Everaers et al.[5,34] introduced a primitive path analysis (PPA) of entanglements where contour reduction is achieved through minimization of an elastic energy. Topology conservation is ensured by treating chains as repulsive objects interacting through an interchain force field. Chain thickness is kept constant throughout this scheme. A modified elastic energy proportional to the chain contour has been used in ref 41 in order to switch from energy minimization to a form of length minimization. In PPA contours are reduced to their final states (PPs) by a combination of contour shrinkage and interchain slipping motion (because of repulsive forces). The latter motion is absent in CReTA, thanks to the adoption of a geometric coarse-graining scheme that leaves out energetics. We have applied our own version of PPA based on a direct numerical minimization of energy, and not on the original molecular dynamics scheme[5,34] (which is a kind of simulated annealing). We have found that interchain slippage results in clustering of TCs in the reduced states. Chains are subjected to tensions which force TC sliding along chain contours up to the point that tensions and repulsions are balanced. Depending on geometry, some TCs close to chain ends are also lost due to TC slippage. TC clustering and the large excluded volume results in a large number of interchain contacts in places where TCs apply. Thus, resolving the topology in terms of individual TCs, and finally reducing the configuration to a network with specified connectivity and nodal points becomes practically intractable. In PPA, reduced configurations are analyzed mainly by what we call "Kuhn mapping" approach, which was introduced as a means of extracting topological measures within PPA. Applications of PPA are described in the Introduction (section 1).

CReTA and PPA apply different kinds of coarse graining. Both work with a bead representation of chains. Their basic differences, which influence PP conformations, are: (i) Avoidance of interchain slippage in CReTA, due to geometric coarse graining. (ii) Chain thickness remains constant in PPA, while it is gradually reduced to a very small value in CReTA. Quantitative estimations of N_e, d from both approaches are in agreement with experimental estimates.[35] We have also applied CReTA to equilibrated PET coarse-grained configurations[63] with similar predictive success. Thus, the average length L of PPs in the reduced states should be comparable from the two methods. This can happen if the amount of contour reduction is comparable between CReTA and PPA, possibly because TC slippage and chain tension, which are absent in CReTA, are compensated by constant chain thickness within PPA. Reduced chain conformations (PPs) will be different. Moreover, it has been shown[41] that within PPA the PP length distribution is sensitive to the chosen energetics. Thus, in general, different coarse-graining schemes will lead to differences in PP statistics.

Kröger presented[43] the Z algorithm, a shortest multiple disconnected path solution to the problem of PPs. CReTA and Z implement a similar geometric scheme of coarse graining, although in a very different way. Both schemes apply shrinking moves similar to those proposed in previous works concerned with the identification of knots in polymer rings[61] and macromolecular chains.[62] In the field of Knot theory these moves can be viewed as a kind of Reidemeister moves.[65] Both CReTA and Z are capable of generating networks. The main differences are as follows: (i) Z deals with infinitely thin line segments, excluded volume is not explicitly represented. Chain thickness is imposed by adjusting the positions of network nodal points. In CReTA chains have an actual excluded volume, due to the bead representation of chains employed. The infinitely thin chain limit is achieved by gradually reducing total excluded volume and extrapolating to zero (see section 3.2). (ii) When periodic boundary conditions (PBC) apply and the size of the simulation cell is comparable to chain dimensions, Z cannot uniquely identify TCs between a chain and its periodic images.[43,64] In such cases, and in order to eliminate PBC effects, an artificially enlarged supercell formed by repetition of the primary cell in all directions[64] can be used. CReTA fully incorporates PBC by construction and is not influenced by such effects. We note that

a more recent version of Z, Z1, is free of this effect and does not require[64] the use of a supercell. (iii) TC counting in Z is not always symmetrical. "Kinks" on one chain formed against a straight segment of another chain do not result in pairwise associated[43] TCs on the two chains. In CReTA all TCs are pairwise associated with other TCs (entanglements are binary). For this reason, Z will result in less TCs than CReTA for the same system. (iv) Z is expected to be computationally faster than CReTA, due to (i) and to the larger number of degrees of freedom that CReTA deals with. In Z, the degrees of freedom are reduced by the contour reduction process, while in CReTA there is a one-to-one correspondence between beads in the molten and reduced network states. When a supercell should be used, Z has also to deal with more degrees of freedom.

Any approach to the chain shrinking problem can only provide an approximate[4,43] solution to PPs. Topology is fixed only in the case[4] of closed rings. Moreover, assignment of TCs to effective spatial positions and bead indices along chains cannot be unique. In our approach, a melt configuration is reduced to a corresponding network configuration where TCs have specified effective localized positions and bead indices along the chains. By altering the course of the contour reduction process, one can end up with displaced network nodal points, both spatially and along the PPs (different bead indices), for the same melt configuration. To investigate this effect, we have categorized chains into subsets and then reduced the subsets sequentially in arbitrary order. The "worst case" scenario is to shrink chains one by one. "One by one" means that we initially employ random aligning moves only on the first chain, with the other chains kept in their melt configurations. σ is reduced down to its final predefined value, as described in section 2. Then, when the contour length of the first chain can no longer be reduced further, we employ aligning moves on both the first and the second chains. Subsequently, when the contour lengths of the first and the second chain can no longer be reduced, we employ aligning moves on the first, second, and third chains, and so on, until all chains have been reduced to a PP network. The sequence of the chains may be chosen randomly. Although resulting PPs obtained through this procedure may differ from the ones presented in this work, which were obtained by stochastic application of the algorithm everywhere in the simulation box, the statistics obtained at the end are practically the same. We have followed the approach that seems most meaningful, which is to shrink all chains simultaneously.

5. Summary

The general problem we studied is the detection of topological constraints (TCs) existing in a system of chain conformations which are random walks at large length scales. We also have studied how these TCs organize into a network. The systems examined are atomistic representations of polyethylene (PE) and *cis*-1,4-polybutadiene (PB). Small length scales as well as the contour length density, volumetric, structural, conformational, and thermodynamic properties for these systems[44−46] are in excellent agreement with available experimental data.

Following previous work[4,5,43] and the Edwards definition of primitive paths (PPs), we have presented a new algorithm called CReTA, and a general methodology for statistical analysis of linear polymer melt topology. Our algorithm removes chain slack (or stored length) from a polymer system, by using geometric operations which respect uncrossability constraints. Thus, chain conformations are reduced to shortest paths specified by the underlying melt topology. In the context of the tube model, shortest paths correspond to PPs. In our approach, PPs emerge in the interconnected form of an entanglement network. Network nodal coordinates correspond to effective localization points of TCs, and network connectivity defines "who is entangled with whom" and in what sequence. We have characterized polymer topology by analyzing the statistical properties of network ensembles of equilibrated PE and *cis*-1,4 PB atomistic specimens. Common organization properties of topological constraints have been revealed. We have shown quantitatively that entanglement networks of chemically different polymers can be structurally scaled so that the underlying melt topologies are statistically the same.

By inspecting network radial distribution functions, a dilute gas of entanglements is revealed. The distribution of the number of skeletal carbon atoms between successive TCs along a chain is found to have an exponentially decaying tail. By invoking a renewal point process which generates TCs, we were able to describe in a stochastic manner the generation of TCs when shrinking a system of atomistic chains. On the basis of this picture the distribution of the number of TCs per chain becomes asymptotically Gaussian.

Topological measures of entanglement networks have been presented for two different length scales. The mesh scale, defined by the average mesh of generated networks, and the "Kuhn scale" where PP conformations are mapped on random walks. We find that descriptions at the Kuhn scale and the mesh scale do not coincide. The Kuhn scale is in accordance with experimental estimates for the entanglement molecular weight and the tube diameter. This has also been observed in previous works.[5,34,35] However, the mesh scale is connected with a density of TCs which is larger than the one defined by the Kuhn scale. In terms of PP conformations this implies that PPs show some stiffness and are not random walks at the mesh scale of entanglement networks. A chain thickness study of topological measures at the Kuhn scale has also been performed.

CReTA offers the ability to define quantities correlating entanglement networks with corresponding melt configurations. Implementing this idea, we have seen that in general not all TCs are equivalent in the way they restrict chain conformations. Examination of a simple geometrical measure shows that it is possible to address the problem of detecting TCs which are related with persistent chain contacts[57−59] in melt configurations. This feature may prove useful in topological investigations of molecular dynamics trajectories or in deformation simulations.

Acknowledgment. This research forms part of the research program of the Dutch Polymer Institute (DPI), project #430. We are grateful to N. Karayannis, V. Mavrantzas, and P. Gestoso for providing the atomistic polymer samples. We thank R. Hoy, M. Robbins, S. Sukumaran, and M. Kröger for stimulating our chain thickness study, and K. Foteinopoulou, N. C. Karayiannis, V. G. Mavrantzas, and M. Kröger for making their manuscript available to us before publication.

Appendix: Distribution of the Number of Beads in *n* Successive Entanglement Strands

The probability distribution function (pdf) of the number of beads x in an entanglement strand is

$$P(x) = \frac{bc}{c-b}(e^{-bx} - e^{-cx})$$

The Laplace transform $G(s)$ of $P(x)$ is

$$G(s) = \frac{bc}{(b+s)(c+s)}$$

Since in a renewal process successive entanglement events are identically and independently distributed, the pdf of the number of monomers in n successive entanglement strands, $P_n(x)$, is the n-fold convolution of $P(x)$ with itself. It is easier to work with the Laplace transform $G_n(s)$ of $P_n(x)$:

$$G_n(s) = [G(s)]^n = \frac{(bc)^n}{(b+s)^n(c+s)^n}$$

With the help of Laplace transform tables and a little algebra, we can invert $G_n(s)$ to determine $P_n(x)$ for $n = 2, 3, 6, 10$. Specifically, we obtain

$$P_2(x) = \frac{(bc)^2}{(b-c)^3}\,(a(x)(e^{-bx} + e^{-cx}) + 2(e^{-bx} - e^{-cx}))$$

$$P_3(x) = \frac{(bc)^3}{2(b-c)^5}\,([(a(x)-3)^2 + 3]e^{-cx} - [(a(x)+3)^2 - 3]e^{-bx})$$

$$P_6(x) = \frac{(bc)^6}{120(b-c)^{11}}\,(f_6(x)(e^{-bx} + e^{-cx}) + g_6(x)(e^{-bx} - e^{-cx}))$$

where

$$a(x) = (b-c)x$$

$$f_6(x) = 15120a(x) + 420a^3(x) + a^5(x)$$

$$g_6(x) = 30240 + 3360a^2(x) + 30a^4(x)$$

and

$$P_{10}(x) = \frac{(bc)^{10}}{181440(b-c)^{19}}\,e^{-\frac{(b+c)x}{2}}\left(f_{10}(x)\cosh\left[\frac{a(x)}{2}\right] - g_{10}(x)\sinh\left[\frac{a(x)}{2}\right]\right)$$

where

$$f_{10}(x) = 8821612800a(x) + 302702400a^3(x) + 2162160a^5(x) + 3960a^7(x) + a^9(x)$$

$$g_{10}(x) = 17643225600 + 2075673600a^2(x) + 30270240a^4(x) + 110880a^6(x) + 90a^8(x).$$

Supporting Information Available: Two videos showing the contour reduction process when CReTA is applied to a single unentangled chain (the .mpg file) and the reduction of a PE-1000 melt sample to the corresponding reduced network of PPs (the .avi file). This material is available free of charge via the Internet at http://pubs.acs.org.

References and Notes

(1) de Gennes, P. G. *Scaling Concepts in Polymer Physics*; Cornell University Press: Ithaca, NY, 1979.
(2) Doi, M.; Edwards, S. F. *The Theory of Polymer Dynamics*; Oxford University Press: NewYork, 1986.
(3) Edwards, S. F. *Br. Polym. J.* **1977**, *9*, 140−143.
(4) Rubinstein, M.; Helfand, E. *J. Chem. Phys.* **1984**, *82*, 2477−2483.
(5) Everaers, R.; Sukumaran, S. K.; Grest, G. S.; Svaneborg, C.; Sivasubramanian, A.; Kremer, K. *Science* **2004**, *303*, 823−826.
(6) Masubuchi, Y.; Ianniruberto, G.; Greco, F.; Marrucci, G. *J. Chem. Phys.* **2003**, *119*, 6925−6930.
(7) Terzis, A. F.; Theodorou, D. N.; Stroeks, A. *Macromolecules* **2002**, *35*, 508−521.
(8) Termonia, Y. *Macromolecules* **1991**, *24*, 1128−1133.
(9) Benkoski, J. J.; Fredrickson, G. H.; Kramer, E. J. *J. Polym. Sci., Part B: Polym. Phys.* **2002**, *40*, 2377−2386.
(10) Meijer, H. E. H.; Govaert, L. E. *Prog. Pol. Sci.* **2005**, *30*, 915−938.
(11) Haward, R. N., Young, R. J., Eds.; *Physics of Glassy Polymers*, 2nd ed.; Chapman & Hall: London, U.K., 1997.
(12) Richter, D.; Farago, B.; Butera, R.; Fetters, L. J.; Huang, J. S.; Ewen, B. *Macromolecules* **1993**, *26*, 795−804.
(13) Ferry, J. D. *Viscoelastic Properties of Polymers*; Wiley: New York, 1986.
(14) Graessley, W. W.; Edwards, S. F. *Polymer* **1981**, *22*, 1329−1334.
(15) Colby, R. H.; Rubinstein, M. *Macromolecules* **1992**, *25*, 996−998.
(16) Lin, Y. H. *Macromolecules* **1987**, *20*, 3080−3083.
(17) Kavassalis, T. A.; Noolandi, J. *Phys. Rev. Lett.* **1987**, *59*, 2674−2677.
(18) Fetters, L. J.; Lohse, D. J.; Richter, D.; Witten, T. A.; Zirkel, A. *Macromolecules* **1994**, *27*, 4639−4647.
(19) Fetters, L. J.; Lohse, D. J.; Graessley, W. W. *J. Polym. Sci., Part B: Polym. Phys.* **1999**, *37*, 1023−1033.
(20) Heynmans, N. *Macromolecules* **2000**, *33*, 4226−4234 and references therein.
(21) Milner, S. T. *Macromolecules* **2005**, *38*, 4929−4939.
(22) Watanabe, H. *Prog. Pol. Sci.* **1999**, *24*, 1253−1403 and references therein.
(23) McLeish, T. C. B. *Adv. Phys.* **2002**, *51*, 1379−1527 and references therein.
(24) Iwata, K.; Edwards, S. F. *Macromolecules* **1988**, *21*, 2901−2904.
(25) Richter, D.; Monkenbusch, M.; Arbe, A.; Colmenero, J. *Adv. Polym. Sci.* **2005**, *174*.
(26) Theodorou, D. N. In *Bridging Time Scales: Molecular Simulations for the Next Decade*; Nielaba, P.; Mareschal, M., Ciccotti, G., Eds.; Springer-Verlag: Berlin, 2002.
(27) Kremer, K. In *Computational Soft Matter: From Synthetic Polymers to Proteins*; Attig. N., Binder, K., Grubmüller, H., Kremer, K., Eds.; NIC Lecture Notes 23; NIC: Jülich, Germany, 2004.
(28) Kröger, M.; Ramírez, J.; Öttinger, H. C. *Polymer* **2002**, *43*, 477−487; Kröger, M. *Models for Polymeric and Anisotropic Liquids*; Springer: Berlin, 2005.
(29) Harmandaris, V. A.; Mavrantzas, V. G.; Theodorou, D. N.; Kröger, M.; Ramírez, J.; Öttinger, H. C.; Vlassopoulos, D. *Macromolecules* **2003**, *36*, 1376−1387.
(30) Padding, J. T.; Briels, W. J. *J. Chem. Phys.* **2004**, *20*, 2996−3002.
(31) Evans, K. E.; Edwards, S. F. *J. Chem. Soc., Faraday Trans. 2* **1981**, *77*, 1913−1927.
(32) Needs, R. J.; Edwards, S. F. *Macromolecules* **1983**, *16*, 1492−1495.
(33) Helfand, E.; Pearson, D. S. *J. Chem. Phys.* **1983**, *79*, 2054−2059.
(34) Sukumaran, S. K.; Grest, G. S.; Kremer, K.; Everaers, R. *J. Polym. Sci., Part B: Polym. Phys.* **2005**, *43*, 917−933.
(35) Leon, S.; van der Vegt, N.; Delle Site, L.; Kremer, K. *Macromolecules* **2005**, *38*, 8078−8092.
(36) Tzoumanekas, C.; Theodorou, D. N. cond-mat/0602555.
(37) Theodorou, D. N. To appear in *Computer Simulations in Condensed Matter: From Materials to Chemical Biology*; Binder, K., Ciccotti, G., Ferrario, M., Eds.; Springer: Berlin, 2006.
(38) Cox, D. R.; Isham, V. *Point Processes*; Chapman and Hall: London, 1980.
(39) Cox, D. R. *Renewal Theory*; Methuen & Co.: London, 1962.
(40) Shanbhag, S.; Larson, R. G. *Phys. Rev. Lett.* **2005**, *94*, 76001.
(41) Zhou, Q.; Larson, R. G. *Macromolecules* **2005**, *38*, 5761−5765.
(42) Hoy, R. S.; Robbins, M. O. *Phys. Rev. E* **2005**, *72*, 61802.
(43) Kröger, M.; *Comput. Phys. Commun.* **2005**, *168*, 209−232.
(44) Karayiannis, N. C.; Mavrantzas, V. G.; Theodorou, D. N. *Phys. Rev. Lett.* **2002**, *88*, 105503.
(45) Karayiannis, N. C.; Giannousaki, A. E.; Mavrantzas, V. G.; Theodorou, D. N. *J. Chem. Phys.* **2002**, *117*, 5465−5479.
(46) Gestoso, P.; Nicol, E.; Doxastakis, M.; Theodorou, D. N. *Macromolecules* **2003**, *36*, 6925−6938.
(47) Uhlherr, A.; M. Doxastakis, M.; Mavrantzas, M. N.; Theodorou, D. N.; Leak, S. J.; Adam, N. E. *Europhys. Lett.* **2002**, *57*, 506−511.
(48) Auhl, R.; Everaers, R.; Grest, G. S.; Kremer, K.; Plimpton, S. J. *J. Chem. Phys.* **200**3, *24*, 12718−12728.
(49) In this case, when σ_f is too small, the protocol for checking bead overlaps has to be changed.
(50) Pearson, D. S.; Strate, G. V.; Meerwall, E. V.; Schilling, F. C. *Macromolecules* **1987**, *20*, 1133−1141.
(51) Greco, F. *Phys. Rev. Lett.* **2002**, *88*, 108301.
(52) Greco, F. *Macromolecules* **2004**, *37*, 10079−10088.
(53) Schieber, J. D. *J. Chem. Phys.* **2003**, *118*, 5162−5166.
(54) des Cloizeaux, J. *J. Phys. I Fr.* **1993**, *3*, 61−68. des Cloizeaux, J. *J. Phys. I Fr.* **1993**, *3*, 1523−1539. des Cloizeaux, J. *J. Phys. I Fr.* **1993**, *4*, 539−550.

(55) Beltzung, M.; Picot, M.; Herz, J. *Macromolecules* **1984**, *17*, 663−669.
(56) See Supporting Information available to this work at http://pubs.acs.org.
(57) Gao, J.; Weiner, J. H. *J. Chem. Phys.* **1995**, *103*, 1621−1626.
(58) Ben-Naim, E.; Grest, G. S.; Witten, T. A.; Baljon, A. R. C. *Phys. Rev. E* **1996**, *53*, 1816−1822.
(59) Yamamoto, R.; Onuki, A *Phys. Rev. E* **2004**, *70*, 41801.
(60) Kremer, K.; Grest, G. S. *J. Chem. Phys.* **1990**, *92*, 5057−5086.
(61) Koniaris, K.; Muthukumar, M. *Phys. Rev. Lett.* **1991**, *66*, 2211−2214.
(62) Taylor, W. R. *Nature* **2000**, *406*, 916−919.
(63) Kamio, K.; Moorthi, K.; Theodorou, D. N. in preparation.
(64) Foteinopoulou, K.; Karayiannis, N. C.; Mavrantzas, V. G.; Kröger, M. *Macromolecules*, in press.
(65) Reidemeister, K. *Abh. Math. Sem. Univ. Hamburg* **1927**, *5*, 7−23.
(66) Shanbhag, S.; Larson, R. G. *Macromolecules* **2006**, *39*, 2413−2417.

MA0607057